CHAPTER 4

Results and discussion (part I) : Preparation and characterizations of BCZT system

In this chapter, the results of characterizations of $Ba_{0.85}Ca_{0.15}Zr_{0.1}Ti_{0.9}O_3$ (BCZT) powders in terms of, chemical bonding and phase formation are firstly mentioned. The result of crystal structure determination of BCZT powders is subsequently introduced. Consequently, the result of phase formation, microstructure, physical properties and electrical properties determinations of the BCZT ceramics are demonstrated.

4.1 BCZT powder preparation

4.1.1 Thermal analysis

Figure 4.1 shows thermal behaviors of $Ba_{0.85}Ca_{0.15}Zr_{0.1}Ti_{0.9}O_3$ powders prepared from solutions with different pH values using TGA-DSC analysis with a constant heating rate of 10°C/ min. The TGA graphs showed weight loss (~8%) for pH5 and pH9 powders while pH7 powder presented the weight loss around 5% in a temperature range of 25 to 188°C, which were believed to be the evaporation of the residual non-structural water and solvents [65, 66]. At the same temperature range, the DSC graphs showed an endothermic peak, which was correlated to the decomposition of water and solvents in the BCZT powders. The second weight loss of 40% (pH5) and 30% (pH9) was observed between 200 to 488°C while the pH7 presented the second weight loss of 13% observed in the temperature range of 200 to 750°C. These weight losses were corresponded to an endothermic and an exothermic peak in the DSC curves which were correlated to a destruction of xerogel network and the successive loss of organic substance [65]. The third weight loss of 10% (pH5 and pH9) at the temperature from 488 to 930°C and 7% (pH7) in the temperature range between 750 to 850°C were related to the elimination of

carbon monoxide (CO) and carbon dioxide (CO_2) molecules and the combustion reactions. These results showed a large endothermic peak. For pH5 and pH9, these peaks showed weight loss of 10% up to the temperature of 1000°C and the TGA graphs still decreased at the temperature more than 1000°C, while pH7 exhibited no significant weight loss above 900°C, which may be correlated to the crystallization process for the powder. The calcination temperature of 900°C was therefore used for BCZT powder preparation.

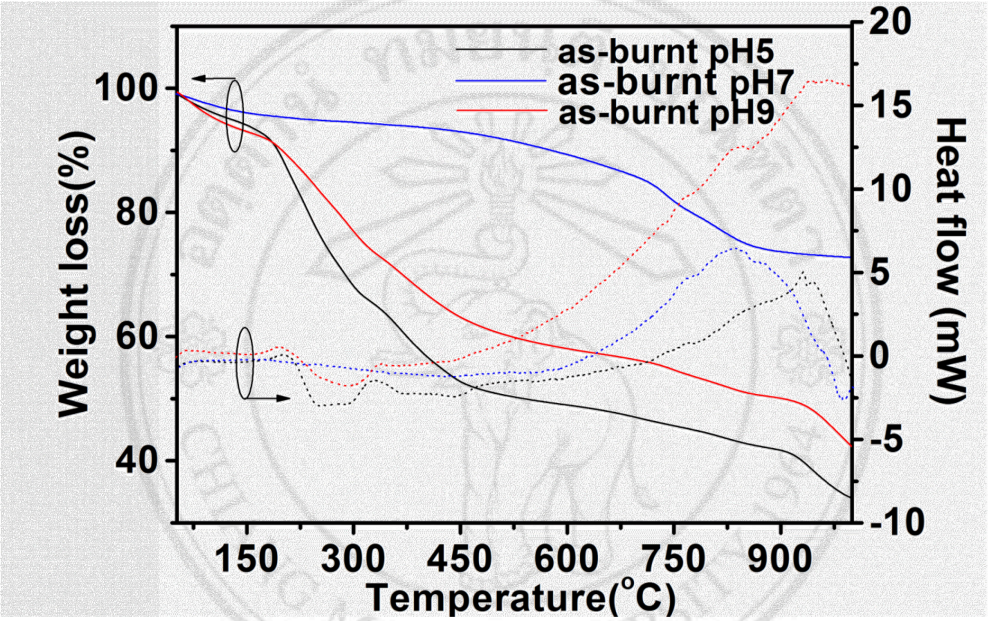

Figure 4.1 Thermal behaviors of as-burnt powders with different pH values.

4.1.2 Structure and phase evolution

Figure 4.2 presents XRD patterns of as-burnt and calcined BCZT powders synthesized by sol-gel auto-combustion method. Some crystalline impurity phases were detected for as-burnt pH 5 powder while as-burnt pH 7 and pH 9 powders exhibited dominant amorphous phase. After calcined at 900°C for 2 h, a pure perovskite phase was observed in the XRD patterns of all calcined powders. The calcination temperature used in this work was lower than those used in conventional mixed oxide method in previous reports [15, 16, 48]. It was found from this present work that powders in nanometer size could be produced by wet chemical methods such as sol-gel [58] and solution auto combustion method [59].It was believed that this viable nanopowder production method occurrable

due to the reduction of external energy from self-propagating combustion mechanism [67]. A broad peak at $2\theta = 45°$ was observed in the XRD patterns which corresponding to Ca^{2+} (A-site) ion diffusing into Ba^{2+} (A-site) and Zr^{4+} (B-site) ions also substituting into Ti^{4+} (B-site), respectively, to form a randomly distributed solid solution. The particle sizes were estimated by using Scherrer's equation [68],

$$t = (0.9\lambda) / (\beta\cos\theta) \quad (4.1)$$

where t is the particle size,

λ is X-ray wavelength which is equal to 1.54178 Å

θ is the collected angle at highest intensity peak,

β is the full width at half maximum (FWHM) of the peak.

The particle sizes of BCZT powders increased from 32 to 35 nm when pH value increased from 5 to 9. It is believed that the chemical reaction of powder's surfaces increased with an increasing of NH_4OH solution content, leading to the agglomeration of the powders.

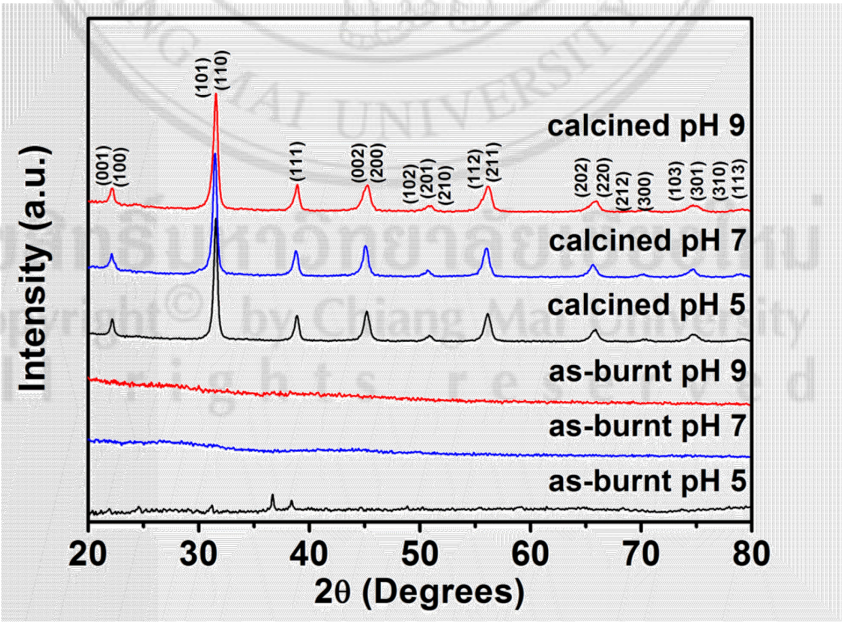

Figure 4.2 XRD patterns of BCZT as-burnt and calcined powders with various pH values.

Figure 4.3 shows the Raman spectra of as-burnt and calcined BCZT powders. For the as-burnt powders prepared from the solution with different pH values, the observed peaks at 1325 and 1588 cm^{-1} were related to disordered of carbon (D-band) and ordered graphitic carbon (G-band), respectively, which confirmed an amorphous structure. There were five Raman active modes which were similar to those observed in $BaTiO_3$. The transverse optical mode (TO) of A1 symmetry and Ti-O bond were observed at the peaks of 181, 182, 186, 239, 245, 247, 251, 301, 302 and 304 cm^{-1}, respectively [58]. The lower peaks frequency presented at 301 and 302 cm^{-1} than $BaTiO_3$ at 304 cm^{-1} and corresponded to B1 and E [TO and longitudinal optical mode (LO)] modes, respectively. These results were supported by a previous report [58]. With an increase in pH value, the peaks at 301 cm^{-1} and 302 cm^{-1} for pH 5, 7 and 9 presented the tetragonality increase. This could be caused by the increase in particle size of powder [69]. The higher intensity and frequency peaks were observed at 714, 718, 721 and 723 cm^{-1}, which were related to A1 (LO), E (LO) modes and the tetragonal phase of BCZT [65]. The peaks at 822, 824, 826, 877, 1062 and 1065 cm^{-1} were also believed to be result of the complete solid solution condition of BCZT powders.

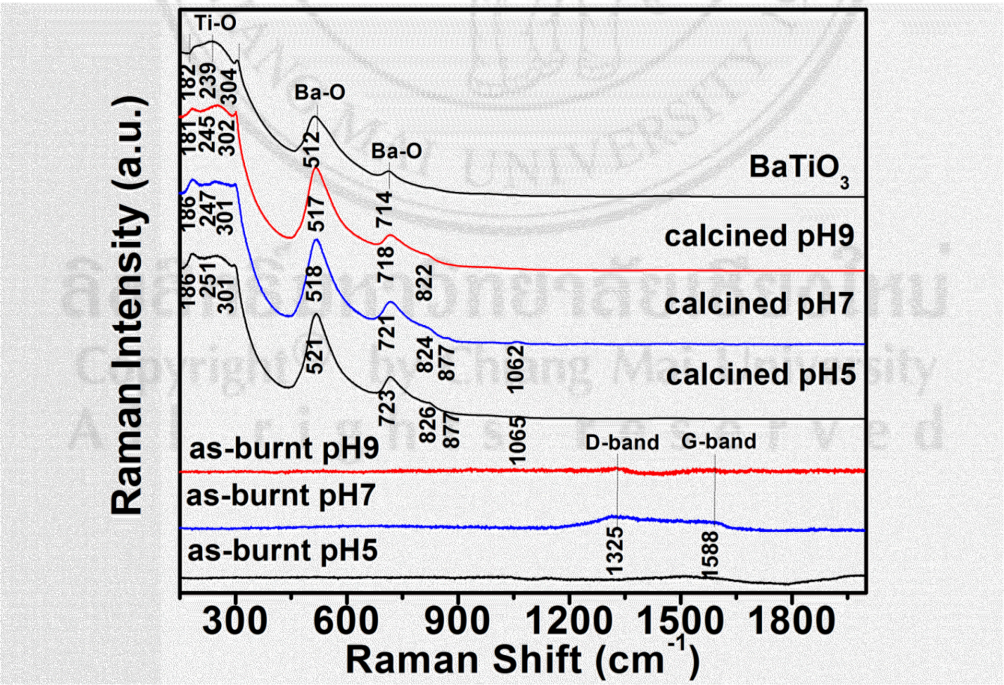

Figure 4.3 Raman spectrums of BCZT as-burnt, BCZT calcined and $BaTiO_3$ powder.

The fourier transform infrared spectra (FTIR) of BCZT as-burnt and calcined powders at various pH values are displayed in Fig. 4.4. The FTIR spectrum for $BaTiO_3$ powder is also shown for comparison. All FTIR peaks of as-burnt and calcined BCZT powders showed broad peak at 3100 to 3700 cm^{-1} corresponding to O-H stretching group of water and citric acid [58, 70, 71, 72]. It was thought that the surface of BCZT powder adsorbed water from the environment which was in good agreement with a previous report [72]. The peaks at 2367-2374 cm^{-1} were assigned to the adsorbed CO_2 molecules from atmosphere [73]. At pH value of 7, the as-burnt and calcined BCZT powder showed peaks at 1715, 1741, 1710 and 1742 cm^{-1} which corresponded to the C-O stretching [58]. The peaks between 1652–1656 cm^{-1} was detected which was corresponded to the bending vibration mode of adsorbed H_2O [72]. The nitrate from raw materials showed the N-O stretching and bending modes in all as-burnt BCZT powders due to the appearance of the peaks at 1568, 1383, 856 and 818 cm^{-1} for pH 5, at 1559, 1375, 857 and 691 cm^{-1} for pH 7 and at 1560, 1380 and 854 cm^{-1} for pH 9 powders [58, 59]. The degree of stretching vibration mode of the carboxylic group (C-O) decreased with increasing pH value and corresponding to the peaks at 1229, 1217, 1215, 1073, 1071 and 1068 cm^{-1} of all as-burnt BCZT powders. The peak at 944 cm^{-1} observed in the as-burnt BCZT powder with pH 5 was related to C-O-H bending vibration which was in agreement with previous work [58]. The peaks at 727, 774, 780, 691 and 688 cm^{-1} indicated metal-oxygen bond [73]. The broad peaks at 558 and 549 cm^{-1} were present in all as-burnt BCZT powders. In addition, the relatively high-intensity FTIR spectra decreased with increasing of pH values which showed the peaks at 553 and 650 for pH 5, 548 and 636 for pH 7, and at 541 and 639 cm^{-1} for pH 9, conditions were observed in the calcined powders while increased as compared to those of $BaTiO_3$. These results correlated to the Ca^{2+} and Zr^{4+} ions substituted into both of Ba^{2+} and Ti^{4+} ions, respectively, which were also supported by Raman spectra [58, 59].

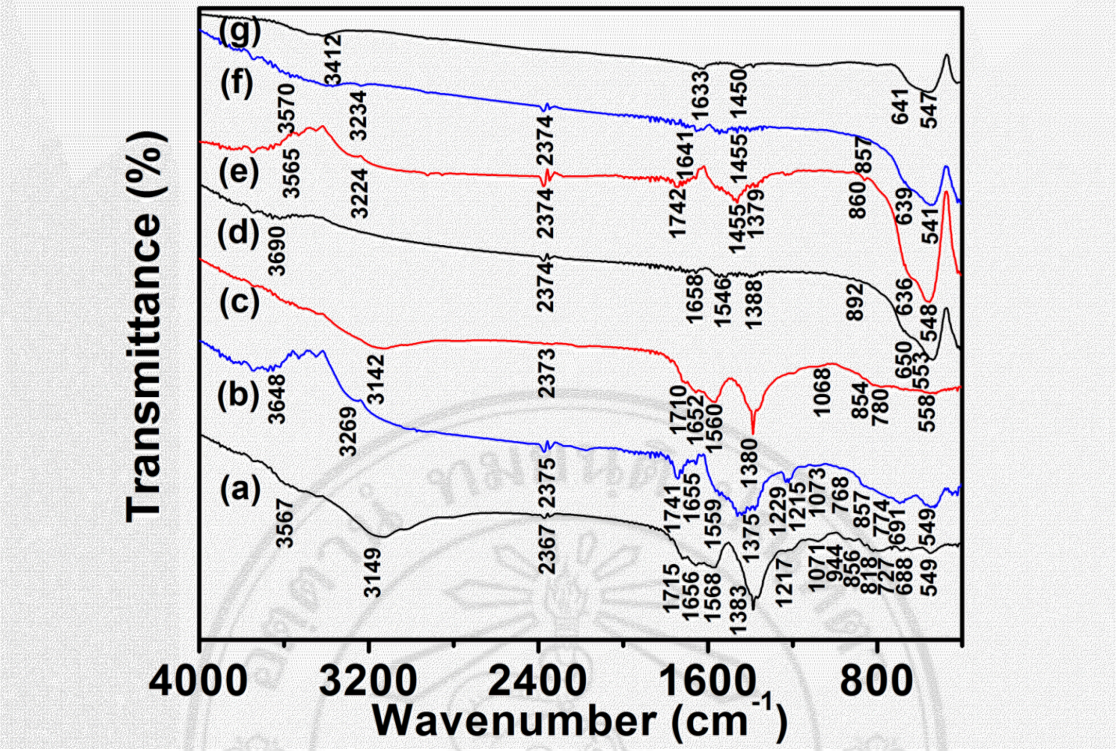

Figure 4.4 Fourier transform infrared spectra of BCZT as-burnt powders with different pH values (a) pH5 (b) pH7 (c) pH9 and calcined powder with various pH values of (d) pH5 (e) pH7 (f) pH 9 and (g) $BaTiO_3$ powder.

4.1.3 Microstructure

Microstructures of the calcined BCZT powders obtained from solution with various pH values observed using scanning electron microscopy (SEM) and transmission electron microscopy (TEM) are shown in Fig. 4.5 and 4.6, respectively. The results showed that most of the particles had a spherical shapes the particle size was in a range of 29-45 nm and 32-35 nm, for SEM and TEM investigations, respectively. The particle size increased with increasing pH values, as given in Table 4.1. An addition of a higher NH_4OH solution content could improve the grain growth behavior. The result was consistent with the XRD result. SAED patterns of calcined BCZT powders are shown in Fig. 4.6(2). The crystal planes could be indexed as (001), (101), (110), (111), (112), (211), (002) and (200) for the BCZT powders calcined at 900 and pH of 5, 7 and 9, respectively. All indexed planes in the patterns confirmed the existence of a tetragonal phase. These results were good agreed with the result obtained from Raman and XRD analysis.

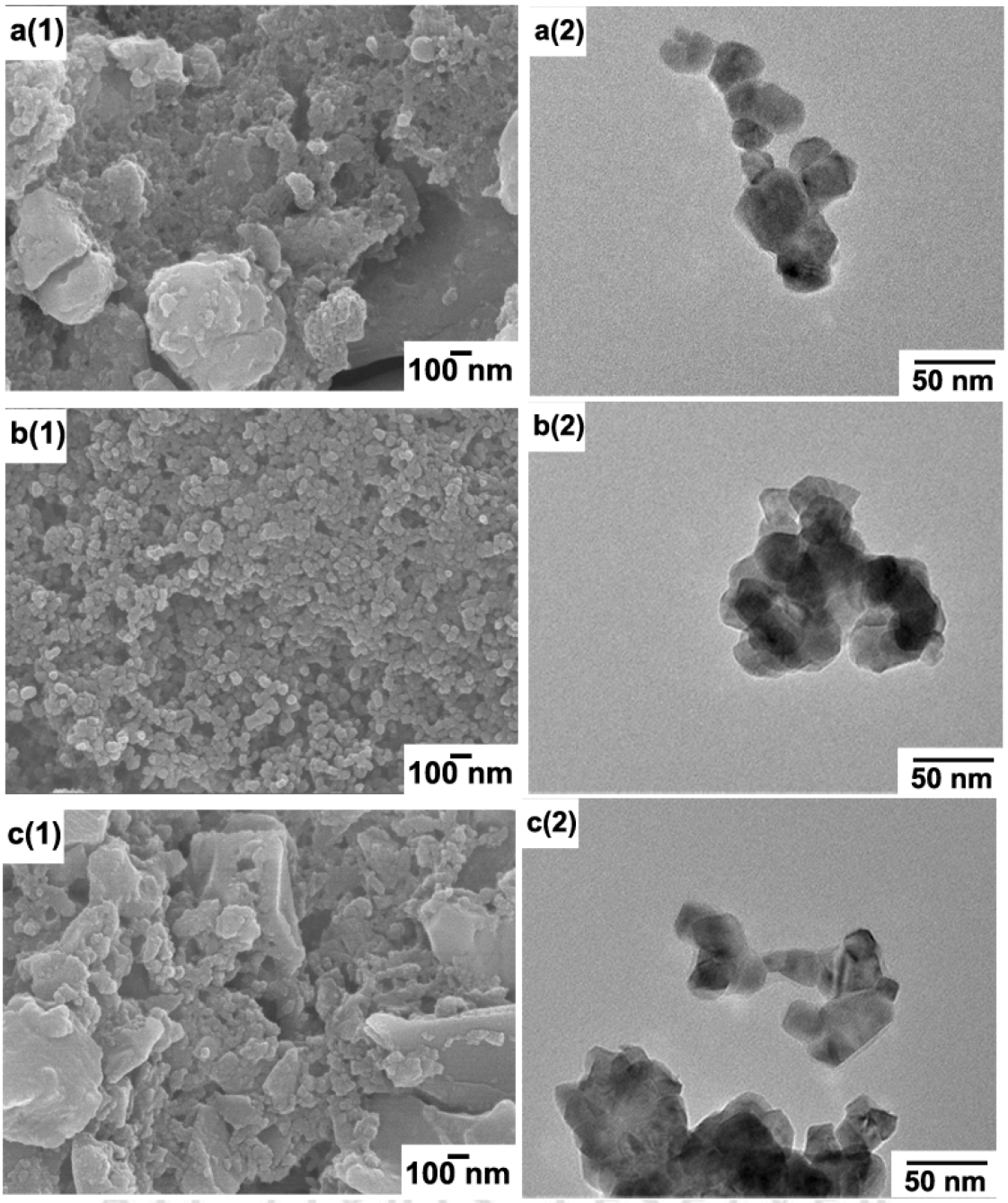

Figure 4.5 SEM (1) and TEM (2) images of BCZT calcined powders with pH values of (a) pH5, (b) pH7 and (c) pH9.

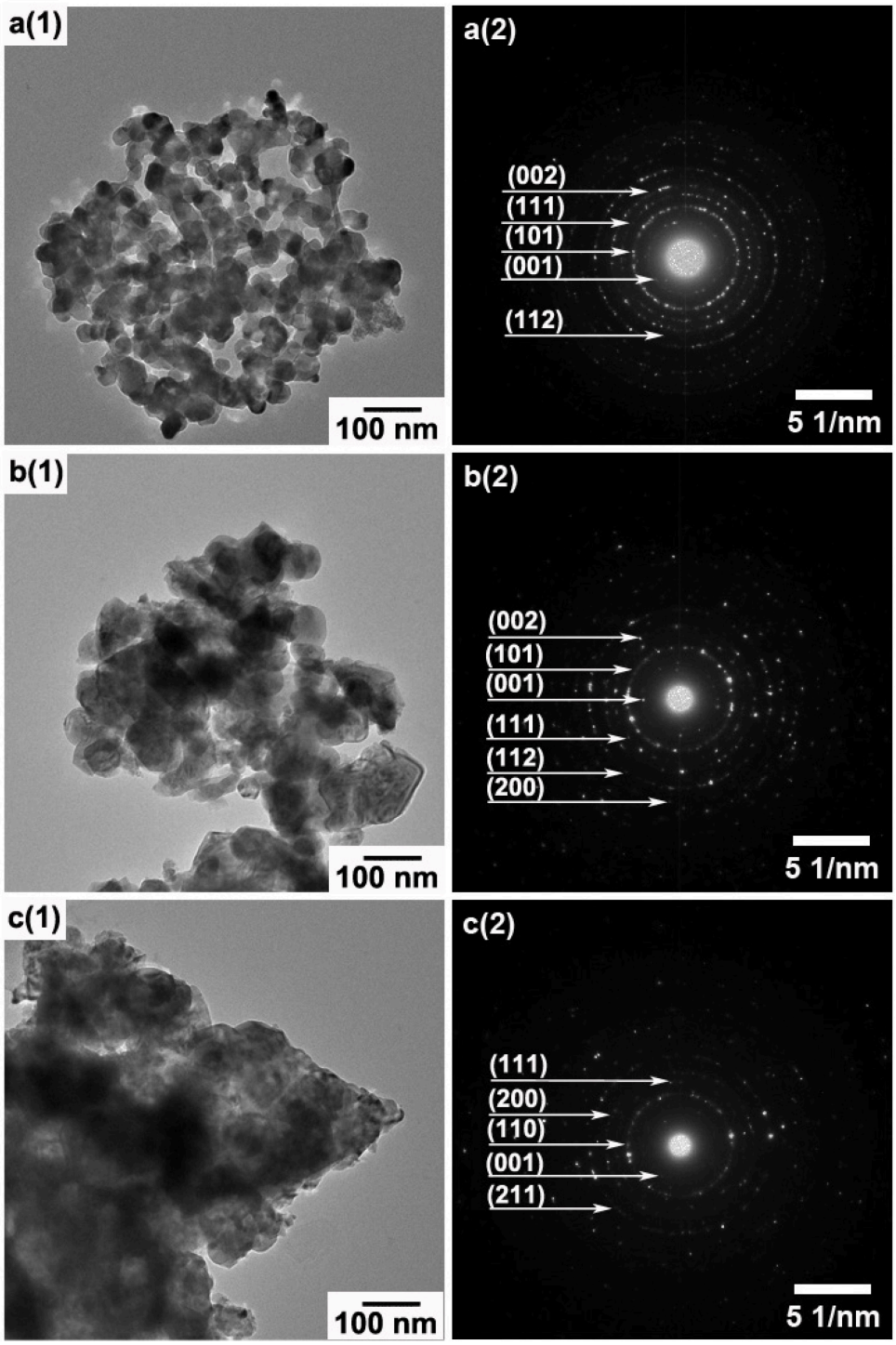

Figure 4.6 TEM images (1) and SAED patterns (2) of BCZT calcined powders with pH values of (a) pH5, (b) pH7 and (c) pH9.

Table 4.1 Average particle sizes obtained from XRD, SEM and TEM results of the BCZT powders with pH values of 5, 7 and 9.

Condition	Average particle size (nm)
XRD	
pH 5	32.16±3.20
pH7	33.68±4.84
pH9	35.23±2.49
SEM	
pH 5	29.88±5.41
pH7	38.23±4.16
pH9	45.09±8.39
TEM	
pH 5	32.51±9.19
pH7	34.24±2.70
pH9	35.07±7.45

4.1.4 Crystal structure

The powder obtained from the optimum condition was used for the crystal structure refinement using Powder Cell Software [74]. The fitting result between calculated and experiment patterns is shown in Fig.4.7. For the Rietveld refinement, Ba and Ca ions were assumed to share the crystallographic A-site of the perovskite structure. Similarly, Ti and Zr ions were both at the B-site. After fitting, the powders possessed a tetragonal

perovskite structure, which agreed well with a previous report [75]. The general crystal structure data of the powder is given in Table 4.2.

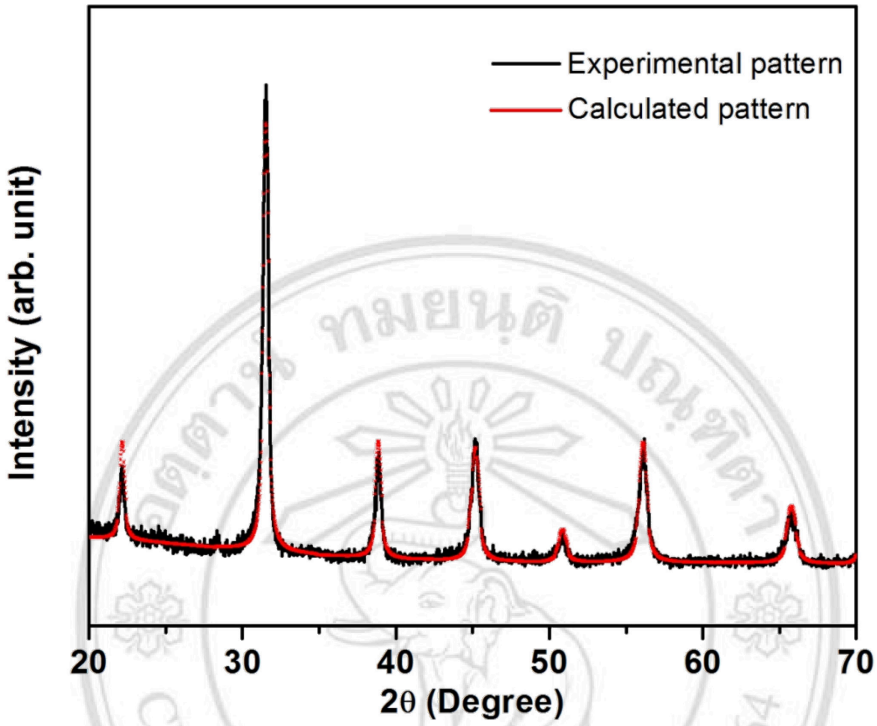

Figure 4.7 The fitting result of the BCZT powder by using Powder Cell Software.

Table 4.2 The crystal structure data of the BCZT powder calcined at 900°C with pH7.

Parameters	**Values**
Space group	P4mm
a = b axis	4.0045 Å
c axis	4.0212 Å
Cell volume	64.4840 $Å^3$
Theoretical density	5.774 g/cm^3

In this study, 900°C was found to be the optimum calcination temperature for BCZT powder which was apparently 400°C lower than those used for the powder prepared by

the mixed oxide method [16, 75]. Although the synthesis temperature was still higher than those employed in citrate sol-gel and solution based auto-combustion methods by about 200 ºC, [76, 77]. Our method was considered to be less complicated in terms of preparation details. In comparison, the citrate sol-gel method required preheating of the gel at 220 ºC for 4 h [78] and the solution based auto-combustion method needed extra time to prepare titanium nitrate from titanium dioxide [77].

4.2 BCZT ceramic preparation

4.2.1 Crystal structure analysis

The BCZT powder calcined at the optimum condition was selected to produce BCZT ceramics sintered at various temperatures from 1200 -1450 ºC for 2 h. Figure 4.8 shows the XRD patterns of BCZT ceramics sintered at various temperatures. A single phase of the perovskite structure was observed in all ceramics. It was possible that Ca^{2+} ions (1.0 Å) could substitute Ba^{2+} ions (1.35 Å), while Zr^{4+} ions (0.72 Å) substituted Ti^{4+} ions (0.68 Å) which agreed with a previous work [10]. The XRD peaks at $2\theta \approx 45^{o}$-46^{o} for (002)/(200) reflections and $2\theta \approx 65^{o}$-67^{o} for (220)/(202) planes indicated an existence of a tetragonal phase. This was consistent with the tetragonal structure observed in BCZT ceramics in previous works [15, 75, 79, 80]. The XRD patterns of the BCZT ceramics sintered at 1400°C and 1450°C were selected to perform refinement using the Powder Cell software. The result as shown in Fig. 4.9 presented the lattice parameters of tetragonal phase with P4mm space group which were found to be a = b (4.012 Å) for 1400°C sample and a = b (4.012 Å) for 1450°C sample. The value of c parameter for both temperatures samples was equal to 4.042 Å. These values were not different even though the sintering temperature was different. The values obtained from the refinement were very close to those reported in the previous works [15, 48].

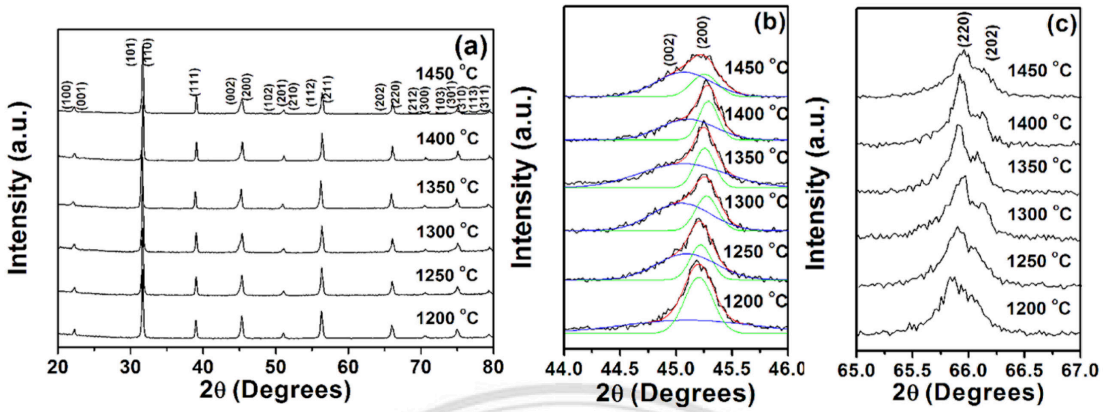

Figure 4.8 XRD patterns of as-burnt and calcined BCZT powders for (a) $2\theta = 20^{o}$-80^{o}, (b) $2\theta \sim 44^{o}$-46^{o} and (c) $2\theta \sim 65^{o}$-67^{o}.

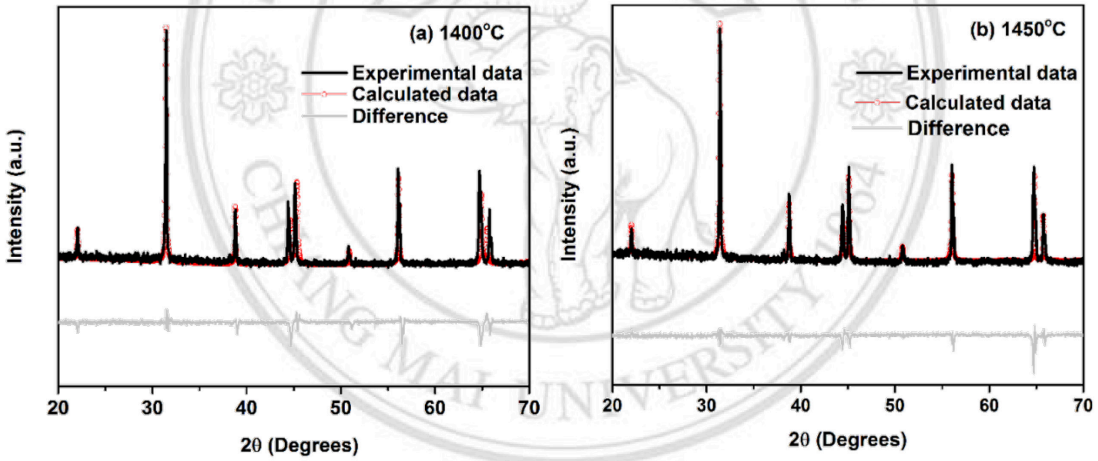

Figure 4.9 Fitting result by Powder Cell Software of BCZT ceramics sintered at (a) 1400°C and (b) 1450°C.

4.2.2 Microstructure and physical properties analysis

Microstructures of surfaces of BCZT ceramics sintered at various temperatures are presented in Fig. 4.10. Average grain sizes of BCZT ceramics increased with increasing sintering temperature. For the ceramics sintered at 1200-1250 the grain sizes were smaller than 1 μm. Above 1250 °C, the grain sizes were found to be in the range of 1.50 to 3.29 μm. SEM images also showed a decreasing trend of porosity of samples with increasing sintering temperature, leading to denser ceramics which was in agreement with

density result. This clearly demonstrated an influence of sintering temperature on controlling grain size of BCZT ceramics [8, 81].

A plot of grain size and density as a function of sintering temperature of BCZT ceramics is shown in Fig. 4.11. Bulk density tended to increase with the increase in sintering temperature from 1200 to 1350 °C. The density did not increase further when sintering temperature is above 1350 °C. The maximum density of BCZT ceramic of 5.60 g/cm^3 obtained in this work was slightly higher than those obtained in Praveen's work (5.52 g/cm^3) [75] and Hao's work (5.53 g/cm^3) [80]. The different density could be explained by a greater homogeneity and a smaller size of BCZT powders prepared in this work.

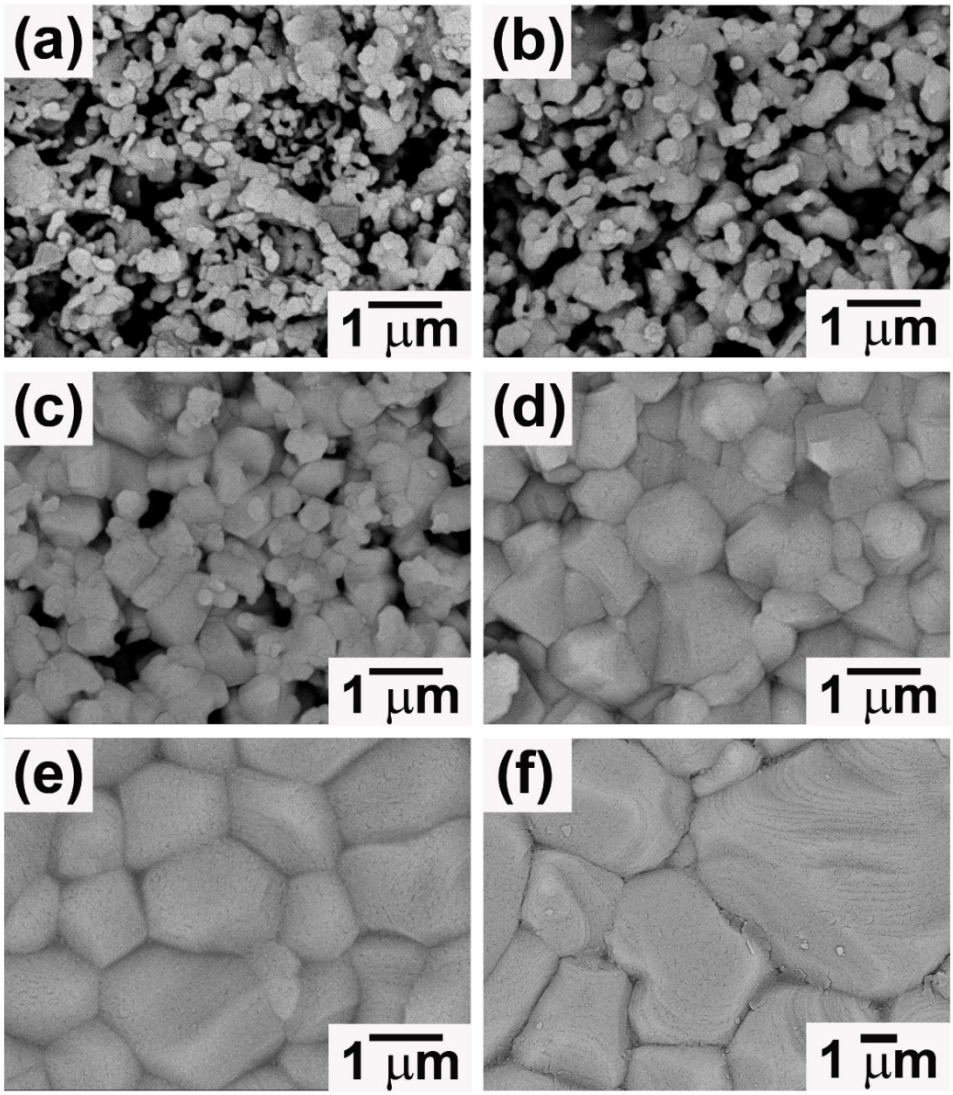

Figure 4.10 SEM images of microstructures of BCZT ceramics sintered at (a) 1200, (b) 1250, (c) 1300, (d) 1350, (e) 1400 and (f) 1450 °C.

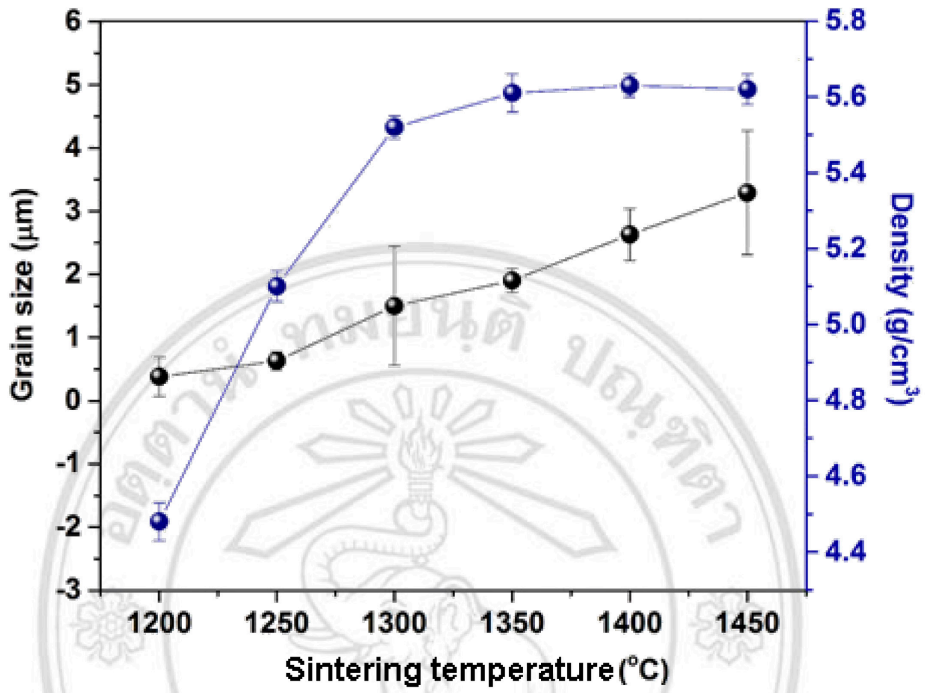

Figure 4.11 Plot of grain size and density as a function of sintering temperature of BCZT ceramics.

The plot of weight loss (%) and shrinkage (%) of BCZT ceramics sintered at different temperatures are shown in Fig. 4.12. It was observed that the weight loss and shrinkage tended to increase with increasing sintering temperature. A higher sintering temperature causes a higher energy for ions to diffuse, making the diffusion of ions easily. This results in a faster grain growth during the initial and intermediate sintering states. These results are good agreement with the grain size and density results as shown in Fig 4.10.

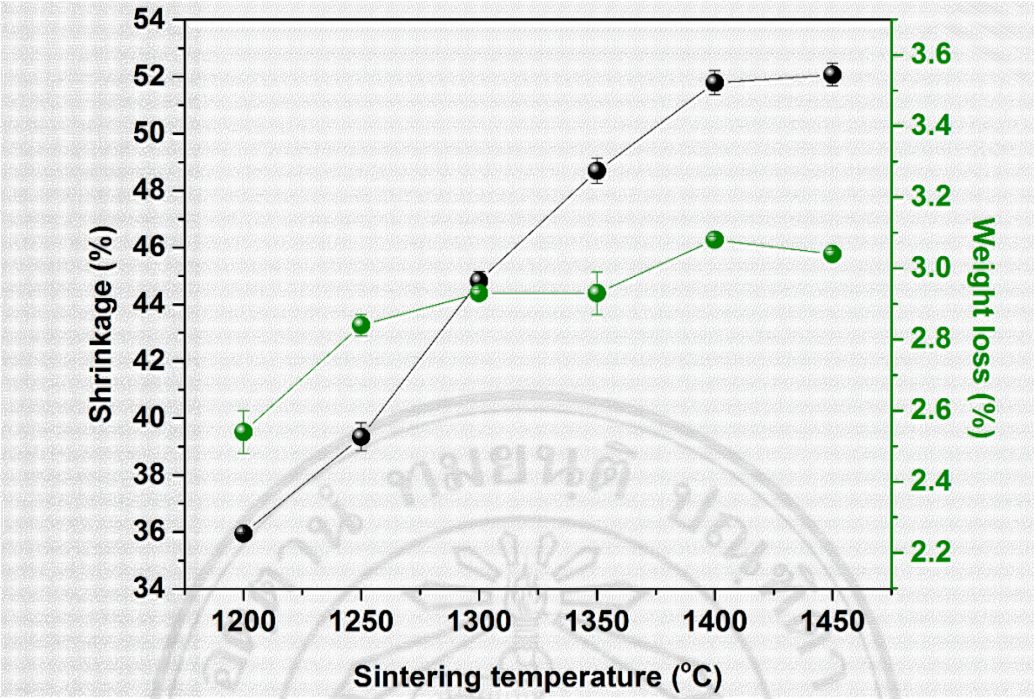

Figure 4.12 Plot of weight loss and shrinkage of BCZT ceramics sintered at various temperatures.

4.2.3 Dielectric properties analysis

Dielectric permittivity (ε_r) and dielectric loss (*tan* δ) measured at room temperature at 1 kHz of BCZT ceramics are shown in Fig. 4.13. The results showed that ε_r values of ceramics tended to increase while *tan* δ decreased with increasing sintering temperature. The BCZT ceramic sintered at 1450 °C exhibited a highest ε_r ~ 5700 and a lowest *tan* δ ~ 0.025. The main factors influencing dielectric properties of ceramics were a high density and a large grain size. When compared with previous work, the ε_r values observed in this work were higher than those in previous reports, which were observed to be about 2000-3500 [15, 48, 79, 80, 82].

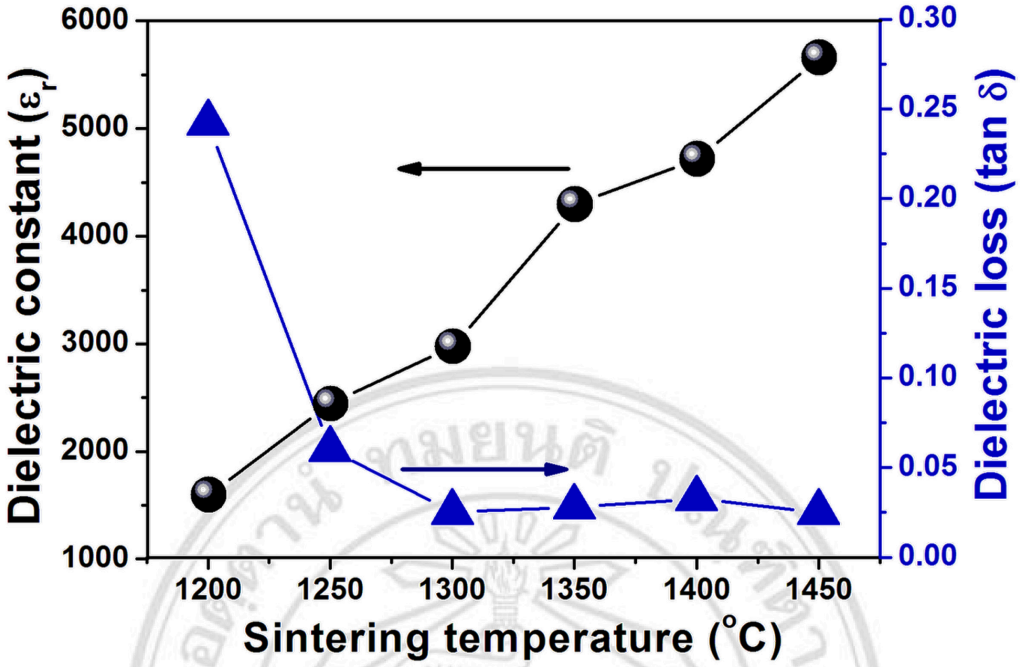

Figure 4.13 Plot of dielectric constant and loss tangent as a function of sintering temperature of BCZT ceramics.

4.2.4 Ferroelectric properties analysis

Figure 4.14 illustrates polarization-electric field (*P-E*) hysteresis loops depicting ferroelectric behaviors of BCZT ceramics sintered at various temperatures. A lossy characteristic was observed in the BCZT ceramic sintered at 1200 °C. This could be caused by the low density of the sample. The *P-E* loops transformed to slim *P-E* loops as the sintering temperature was above 1200 °C. The observed result indicated relaxor behavior of the ceramics [80, 83, 84] with low electric filed required for domain to switch [75]. From Figure 4.15, the remnant polarization (P_r) tended to increase from 0.24 to 1.98 μC/cm^2 for the BCZT ceramics sintered at the temperature ranged from 1300 °C to 1450 °C. The maximum P_r observed in this work was lower than those observed in recent reports [75, 79, 80] which was mainly due to the different of grain sizes. For example, in this study, the BCZT ceramic sintered at 1450 °C showed rather different P_r (1.98 μC/cm^2) and E_c (2.46 kV/cm) values when compared to the samples sintered at the same sintering temperature as reported by Hao *et al.* (P_r > 12 μC/cm^2 and E_c ~ 4 kV/cm) [80]

and Coondoo *et al.* ($P_r \sim 8$ μC/cm^2 and $E_c \sim 4$ kV/cm) [85]. This may be explained by the fact that the average grain size of our sample was 3.3 μm while those of Hao *et al.* [80] and Coondo *et al*. [85] were equal to 10.8 μm and 25 μm, respectively. The coercive field (E_c) showed a significantly decrease with increasing sintering temperature from 1200 to 1300 °C. This was due to the reduced contribution of the space charge response and the more fully developed microstructure at higher sintering temperatures. The low E_c values observed in this study was also in agreement with other works [15, 79]. The small grain size in BCZT system which were in the range of 3-4 μm and showed the relaxor behavior. It has been reported that the small grains have low degree of domain configuration, weakening of long-range ferroelectric interactions and high internal stress which also enhance a relaxor behavior with slim *P-E* loop. These results were are good agreement with the previous works [83, 84, 86, 87].

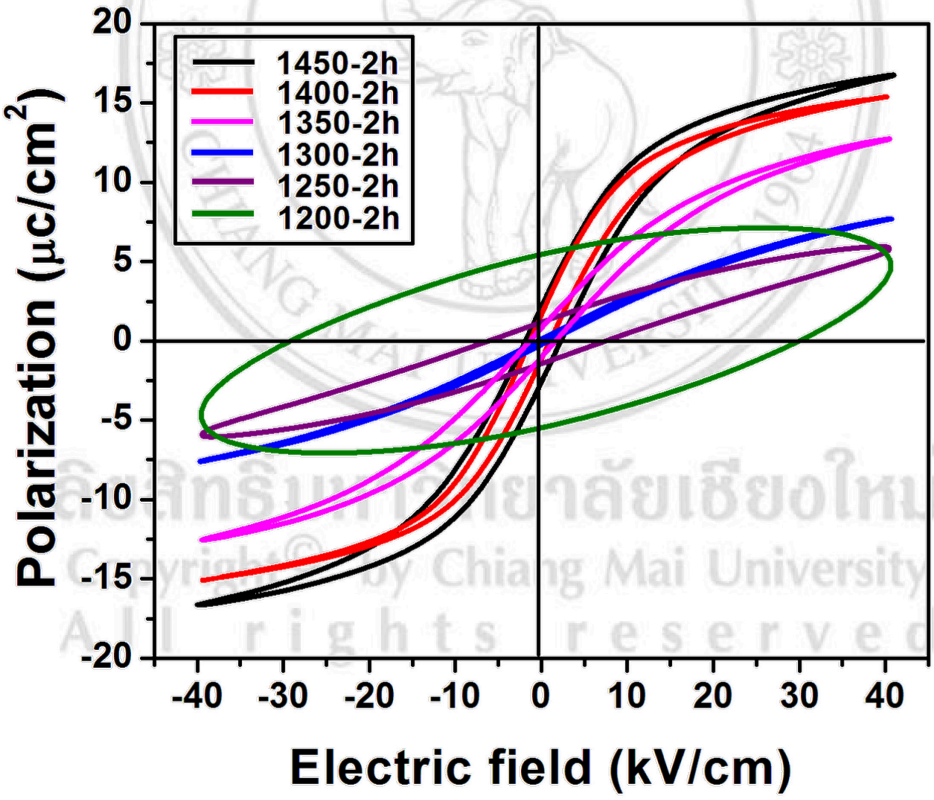

Figure 4.14 *P-E* hysteresis loops of BCZT ceramics sintered at various temperatures.

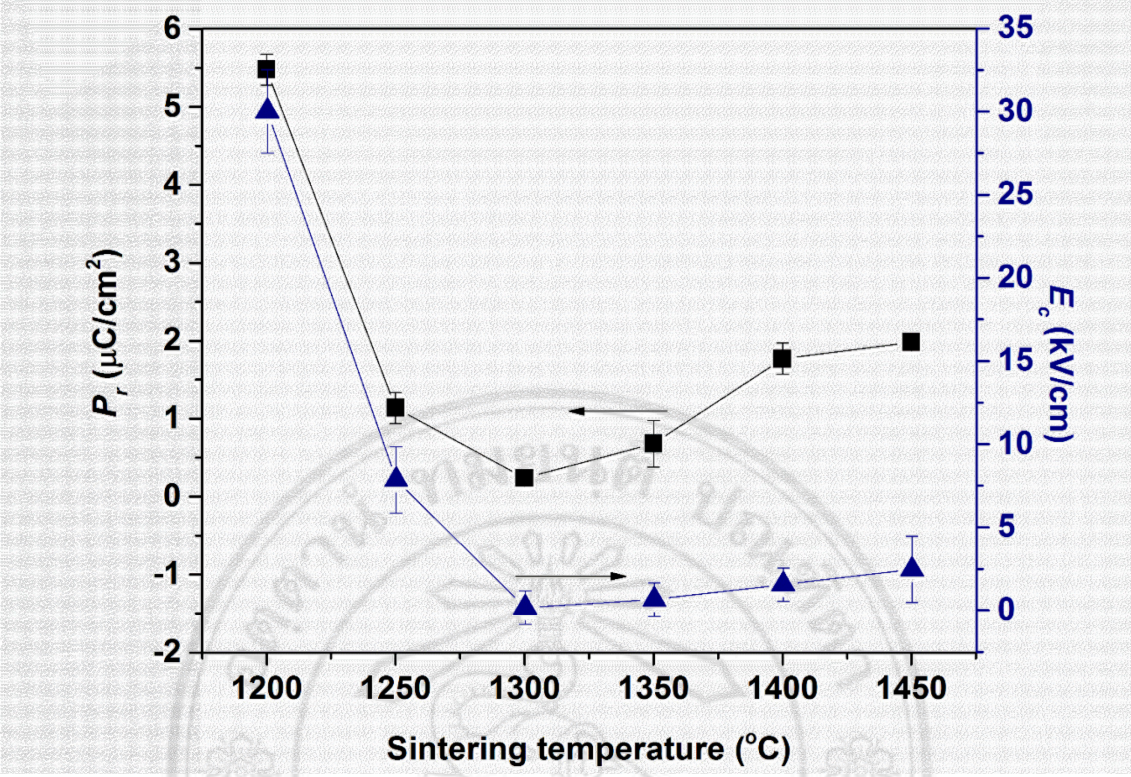

Figure 4.15 Plot of P_r and E_c as a function of sintering temperature of BCZT ceramics.

4.2.5 Electrostrictive properties analysis

Strain (*S*) - Electric field (*E*) relationships of BCZT ceramics are shown in Figure 4.16. Because the BCZT ceramics sintered at 1200-1250 °C were broken down during the measurement, therefore, their electric field-induced strain data could not be obtained. The BCZT ceramic sintered at 1300 °C showed a lowest strain (0.01%) with an unsaturated *S*-*E* loop. The BCZT ceramics sintered at 1350-1400 °C showed greater strain responses due to their higher bulk densities. The *S*-*E* curves with a slim butterfly-like shape and a small positive strain of 0.06% and 0.07% were observed for the samples sintered at 1350 °C and 1400 °C, respectively. A very small negative strain of about 0.02% was also observed for these samples. The BCZT ceramic sintered at 1450 °C presented highest strain of ~0.08% with the disappearance of negative strain.

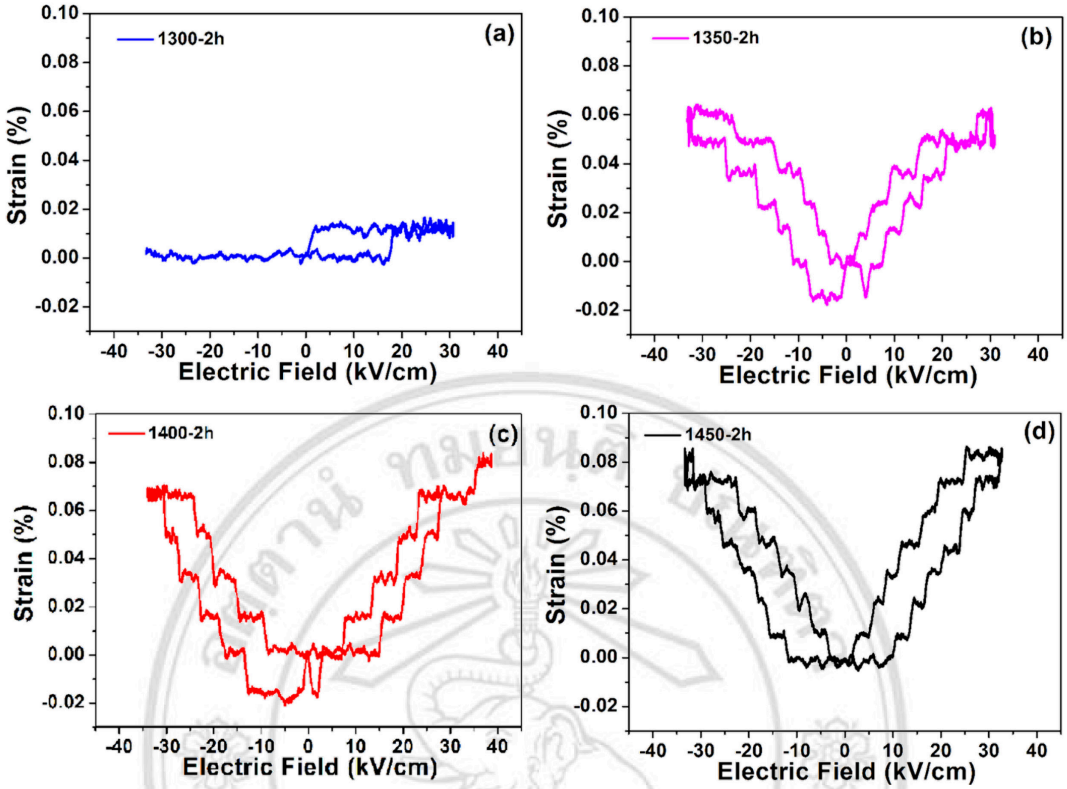

Figure 4.16 Plots of Strain (*S*) - Electric field (*E*) of BCZT ceramics sintered at (a) 1300, (b) 1350, (c) 1400 and (d) 1450 °C.

In this study, BCZT ceramics showed better dielectric permittivity ($\varepsilon_r \sim 5700$) than $BaTiO_3$ (~3000) [88] and soft PZT materials (~2000-3500) [15]. Moreover, electrical properties of these sol-gel auto-combustion derived BCZT ceramics may be improved and tailored by optimizing processing and sintering conditions as well as addition of potential dopants in order for them to be designed for specific applications including electromechanical sensors and actuators.